

2

**Space-Time Structure of the Morning
Aurora Inferred from Coincident DMSP-F6,
-F8, and Søndrestrøm Incoherent Scatter
Radar Observations**

1 October 1993

Prepared by

**J. WATERMANN and O. de la BEAUJARDIÈRE
SRI International
Menlo Park, CA**

and

**H. E. SPENCE
Space and Environment Technology Center
Technology Operations
The Aerospace Corporation**

**DTIC
ELECTE
FEB 04 1994
S B D**

Prepared for

**SPACE AND MISSILE SYSTEMS CENTER
AIR FORCE MATERIEL COMMAND
2430 E. El Segundo Boulevard
Los Angeles Air Force Base, CA 90245**

Engineering and Technology Group

94-03567



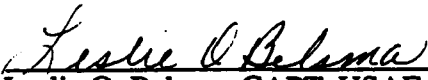
**APPROVED FOR PUBLIC RELEASE;
DISTRIBUTION UNLIMITED**

94 2 02 046

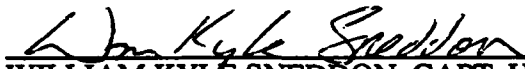
This report was submitted by The Aerospace Corporation, El Segundo, CA 90245-4691, under Contract No. F04701-88-C-0089 with the Space and Missile Systems Center, 2430 E. El Segundo Blvd., Suite 6037, Los Angeles AFB, CA 90245-4687. It was reviewed and approved for The Aerospace Corporation by A. B. Christensen, Principal Director, Space and Environment Technology Center. Capt. Leslie O. Belsma was the project officer for the Mission-Oriented Investigation and Experimentation (MOIE) program.

This report has been reviewed by the Public Affairs Office (PAS) and is releasable to the National Technical Information Service (NTIS). At NTIS, it will be available to the general public, including foreign nationals.

This technical report has been reviewed and is approved for publication. Publication of this report does not constitute Air Force approval of the report's findings or conclusions. It is published only for the exchange and stimulation of ideas.



Leslie O. Belsma, CAPT, USAF
MOIE Program Manager



WILLIAM KYLE SNEDDON, CAPT, USAF
Deputy Chief
Industrial and International Division

REPORT DOCUMENTATION PAGE			Form Approved OMB No. 0704-0188	
Public reporting burden for this collection of information is estimated to average 1 hour per response, including the time for reviewing instructions, searching existing data sources, gathering and maintaining the data needed, and completing and reviewing the collection of information. Send comments regarding this burden estimate or any other aspect of this collection of information, including suggestions for reducing this burden to Washington Headquarters Services, Directorate for Information Operations and Reports, 1215 Jefferson Davis Highway, Suite 1204, Arlington, VA 22202-4302, and to the Office of Management and Budget, Paperwork Reduction Project (0704-0188), Washington, DC 20503.				
1. AGENCY USE ONLY (Leave blank)		2. REPORT DATE 1 October 1993		3. REPORT TYPE AND DATES COVERED
4. TITLE AND SUBTITLE Space-Time Structure of the Morning Aurora Inferred from Coincident DMSP-F6, -F8, and Søndrestrøm Incoherent Scatter Radar Observations			5. FUNDING NUMBERS F04701-88-C-0089	
6. AUTHOR(S) Watermann, J.; de la Beaujardière, O.; and Spence, H. E.				
7. PERFORMING ORGANIZATION NAME(S) AND ADDRESS(ES) The Aerospace Corporation Technology Operations El Segundo, CA 90245-4691			8. PERFORMING ORGANIZATION REPORT NUMBER TR-92(2940)-4	
9. SPONSORING/MONITORING AGENCY NAME(S) AND ADDRESS(ES) Space and Missile Systems Center Air Force Materiel Command 2430 E. El Segundo Blvd. Los Angeles Air Force Base, CA 90245			10. SPONSORING/MONITORING AGENCY REPORT NUMBER SMC-TR-93-63	
11. SUPPLEMENTARY NOTES				
12a. DISTRIBUTION/AVAILABILITY STATEMENT Approved for public release; distribution unlimited			12b. DISTRIBUTION CODE	
13. ABSTRACT (Maximum 200 words) On rare occasions, observations from the DMSP-F6 and -F8 spacecraft and the Søndrestrøm incoherent scatter radar coincide in space. Such coincidence offers a unique opportunity to study temporal vs spatial variations on a small scale. We discuss data from one of those occasions, with observations made in the dawn sector in the presence of moderate auroral precipitation during a magnetically quiet period. The DMSP satellites measured vertical electron and ion flux and cross-track plasma drift while the radar measured the ionospheric electron density distribution and line-of-sight plasma velocities. We combine these data sets to construct a two-dimensional map of a possible auroral pattern above Søndrestrøm. It is characterized by the following properties. No difference is seen between the gross precipitation patterns measured along the DMSP-F6 and -F8 trajectories (separated by 32 km in magnetic east-west direction and some 4 s in travel time in magnetic north-south direction), except that they are not exactly aligned with the <i>L</i> shells. However, F6 and F8 observed minor differences in the small-scale structures. More significant differences are found between small-scale features in the DMSP precipitation measurements and in radar observations of the <i>E</i> -region plasma density distribution. These measurements are separated by 74 km, equivalent to 2.4°, in magnetic longitude, and 0-40 s in time along the spacecraft trajectories (varying with magnetic latitude). Large-scale magnetospheric-ionospheric surfaces such as plasma flow reversal, poleward boundary of the keV ion and electron precipitation, and poleward boundary of <i>E</i> -region ionization, coincide. The combined data suggest that the plasma flow reversal delineates the polar cap boundary, that is, the boundary between precipitation characteristic for the plasma mantle and for the plasma sheet boundary layer.				
14. SUBJECT TERMS Aurora DMSP Particle Precipitation			15. NUMBER OF PAGES 16	
			16. PRICE CODE	
17. SECURITY CLASSIFICATION OF REPORT Unclassified	18. SECURITY CLASSIFICATION OF THIS PAGE Unclassified	19. SECURITY CLASSIFICATION OF ABSTRACT Unclassified	20. LIMITATION OF ABSTRACT	

CONTENTS

ABSTRACT.....	2
1. INTRODUCTION.....	2
2. OBSERVATIONS.....	3
3. DISCUSSION AND CONCLUSIONS	10
REFERENCES.....	12

FIGURES

1. Left: Geographic latitude-longitude grid with the Søndrestrøm incoherent scatter radar and its elevation scan trace, DMSP-F6 and -F8 trajectories, and invariant latitude contours, all mapped to 120 km altitude; Right: enlarged central part of the grid including the radar location and the 0803 UT marks, showing the distances between radar scan trace, F8 trajectory, and F6 trajectory.....	4
2. DMSP-F8 measurements of the number flux of electrons and ions and cross-track plasma drift.....	6
3. Plasma drift in radar scan plane, perpendicular to the geomagnetic field and averaged over 0.6° invariant, from the radar elevation scan simultaneous with the DMSP passes	5
4. Averaged plasma velocity vectors perpendicular to the geomagnetic field inferred from a combination of DMSP-F8 and radar drift measurements, plotted on the same grid as Fig. 1.....	8
5. Ion and electron energy flux measured onboard DMSP-F6 and -F8, synchronized in invariant latitude	7
6. Ionospheric raw plasma density profiles obtained from four consecutive radar elevation scans separated by 4.5 min.....	9
7. A possible interpretation of the combined radar and spacecraft observations plotted on the grid used in Fig. 1.....	11

DTIC QUALITY INSPECTED 8

Accession For	
NTIS GRA&I	<input checked="" type="checkbox"/>
DTIC TAB	<input type="checkbox"/>
Unannounced	<input type="checkbox"/>
Justification	
By.....	
Distribution/.....	
Availability Codes	
Dist	Avail and/or Special
A-1	

Space-time structure of the morning aurora inferred from coincident DMSP-F6, -F8, and Søndrestrøm incoherent scatter radar observations

J. WATERMANN,* O. DE LA BEAUJARDIÈRE* and H. E. SPENCE†

*Geoscience and Engineering Center, SRI International, 333 Ravenswood Avenue, Menlo Park, CA 94025, U.S.A. :

†The Aerospace Corporation, Space and Environment Technology Center, Los Angeles, CA 90009, U.S.A.

Abstract—On rare occasions, observations from the DMSP-F6 and -F8 spacecraft and the Søndrestrøm incoherent scatter radar coincide in space. Such coincidence offers a unique opportunity to study temporal vs spatial variations on a small scale. We discuss data from one of those occasions, with observations made in the dawn sector in the presence of moderate auroral precipitation during a magnetically quiet period. The DMSP satellites measured vertical electron and ion flux and cross-track plasma drift while the radar measured the ionospheric electron density distribution and line-of-sight plasma velocities. We combine these data sets to construct a two-dimensional map of a possible auroral pattern above Søndrestrøm. It is characterized by the following properties. No difference is seen between the gross precipitation patterns measured along the DMSP-F6 and -F8 trajectories (separated by 32 km in magnetic east-west direction and some 4 s in travel time in magnetic north-south direction), except that they are not exactly aligned with the L shells. However, F6 and F8 observed minor differences in the small-scale structures. More significant differences are found between small-scale features in the DMSP precipitation measurements and in radar observations of the E -region plasma density distribution. These measurements are separated by 74 km, equivalent to 2.4° , in magnetic longitude, and 0–40 s in time along the spacecraft trajectories (varying with magnetic latitude). Large-scale magnetospheric-ionospheric surfaces such as plasma flow reversal, poleward boundary of the keV ion and electron precipitation, and poleward boundary of E -region ionization, coincide. The combined data suggest that the plasma flow reversal delineates the polar cap boundary, that is, the boundary between precipitation characteristic for the plasma mantle and for the plasma sheet boundary layer.

1. INTRODUCTION

Coincident high-latitude ground-based and spaceborne measurements of ionospheric plasma parameters have been widely used in the past to study phenomena of magnetosphere-ionosphere coupling in more detail than would be possible from either one alone. Low-altitude spacecraft (orbiting below some 1000 km) are particularly convenient for this purpose. Field line mapping does not pose a problem, because an IGRF model is usually accurate enough and appropriate under various solar wind, magnetospheric, and ionospheric conditions. Auroral electron acceleration is often confined to altitudes above some 1000 km, for example, REIFF *et al.* (1988). Only occasionally significant acceleration is found below 800 km altitude, for example, RINNERT *et al.* (1986). Therefore, precipitation of energetic electrons (tens of eV to tens of keV), observed on low-altitude satellites, corresponds in most cases directly to ionospheric plasma density enhancements. Also, electric fields perpendicular to the magnetic field B_0 are approximately

the same at the spacecraft altitude and in the ionosphere, except for a magnetic field geometry factor.

The combination of coincident measurements from ground and space can enhance the space-time resolution of the observations and may allow mapping between magnetospheric boundaries and their ionospheric signatures, based on physically observable parameters (such as particle characteristics) instead of solely on magnetic field or electrostatic potential models. In this paper we discuss the exceptional case of having a triple set of such measurements, namely from two DMSP (Defense Meteorological Satellite Program) spacecraft (RICH *et al.*, 1985) and from the Søndrestrøm incoherent scatter radar (KELLY, 1983; WICKWAR *et al.*, 1984). Our study is not the first to combine Søndrestrøm radar observations and data from two low-altitude spacecraft. ROBINSON *et al.* (1984) examined coincident observations from the Søndrestrøm radar and from the Triad and NOAA-7 satellites. In a follow-up study, ROBINSON *et al.* (1988) analyzed coincident DMSP-F6, HILAT, and Søndrestrøm radar observations. In those two studies,

the satellites were widely spaced. The authors inferred the development of a large-scale auroral pattern, but small-scale variations could not be resolved. In this paper we examine data acquired simultaneously with two closely spaced low-altitude satellites and the Søndrestrøm radar.

We compare particle precipitation and plasma drift measurements from the SSJ/4 and SSIES instruments on DMSP-F6 and -F8 (RICH *et al.*, 1985) during a pass of the satellites in close formation over western Greenland with complementary ionospheric observations made with the Søndrestrøm incoherent scatter radar almost underneath the spacecraft trajectories. The combined data are used to determine the polar cap boundary, the distribution of the discrete aurora, and the plasma drift pattern in the dawn sector. The small temporal and spatial offsets between the three data sets yield information about the space-time structure of auroral patterns and the polar cap boundary with high resolution (a couple of seconds in time and a few tens of kilometers in magnetic longitude). They also allow us to compile a two-dimensional view of the auroral ionosphere over Søndrestrøm and its association with magnetospheric regions, even in the absence of auroral images.

2. OBSERVATIONS

The Søndrestrøm incoherent scatter radar is located at 67° geodetic latitude and 309° longitude. Its invariant latitude of 73.8° corresponds to $L = 12.8$, and the local contour of constant invariant latitude is rotated between 27° (at ground level) and 26° (at 1000 km altitude) counterclockwise from geographic east. These numbers are computed from the IGRF 1985 model, extrapolated to epoch 1990.3. During the event that we report here, the radar scanned the ionosphere with constant slew rate back and forth in a plane perpendicular to the local L shell. Each elevation scan took 4.5 min except the one preceding the DMSP passes which was stopped about 3 min prior to the satellite passes, before the antenna had reached lowest elevation, in order to synchronize the next scan with the satellite passes. The scan sequence was restarted with the antenna pointing southward at lowest elevation to achieve optimal coincidence with the polebound DMSP passes. The antenna motion was such that the antenna pointed along the field line when the spacecraft crossed the L shell through the radar location. To compensate for the weak radar signal (owing to the generally low ionospheric electron density) we used a fairly long integration time, 20 s corresponding to 30 km spatial integration at 120 km

overhead the radar. The electron density measurements above 120 km altitude were corrected with electron and ion temperatures obtained from fits to the measured spectra.

The DMSP-F6 and -F8 spacecraft move in nearly identical, Sun-synchronous circular orbits at 98° inclination, and they cross the equator near the dawn-dusk meridian. Because of their different altitudes (821 and 865 km, respectively), the spacecraft have slightly different velocities, with the effect that the lower F6 overtakes the higher F8 about once every eleven days. When passing over Søndrestrøm, the spacecraft trajectories happen to cross the contours of constant invariant latitude approximately perpendicularly. Although the F6 spacecraft was officially decommissioned after F8 began operation, simultaneous observations were made during a few periods of close approach between F6 and F8.

The F6 and F8 spacecraft measure charged particle precipitation in the energy range 30 eV–30 keV. Their electron and ion spectrometers are each divided into two channels, sensitive to particles below and above 1 keV, respectively. All four channels are scanned once per second through ten logarithmically spaced energy levels. The spectrometers are always pointing vertically upward, therefore pitch angle distributions cannot be determined. The DMSP-F8 driftmeter provides measurements of the vertical and horizontal cross-track plasma drift.

The sole event for which coincident data from the Søndrestrøm radar and both DMSP spacecraft are available took place on 4 April 1990, between 0801 and 0805 UT. The time corresponds to 6.2 h magnetic local time and 4.7 h solar local time at Søndre Strømfjord. At a solar zenith angle of 93°, the atmosphere was sunlit above 9 km altitude, therefore no auroral images are available to support our interpretation. The event occurred during an extended magnetically quiet period between two magnetic storms commencing 5 days before and 5 days after the event. During the event, the K_p index reached only 2+. IMF data are not available for this time interval. The AFGL ionosonde at Søndrestrøm did not detect F -layer echoes, only echoes from the E -layer with $f_oE \approx 4$ MHz, corresponding to a peak plasma density of $2 \cdot 10^{11} \text{ m}^{-3}$ (Buchau, private commun.). The ionosonde measurements are consistent with the incoherent scatter radar data which identified an E -region peak density of $1.5 \cdot 10^{11} \text{ m}^{-3}$. Despite the geomagnetic quiescence, auroral particle precipitation and small-scale thermal plasma density variations were observed.

The left-hand side of Fig. 1 gives an overview of the geographic configuration of the experiment. The time

Morning aurora space-time structure

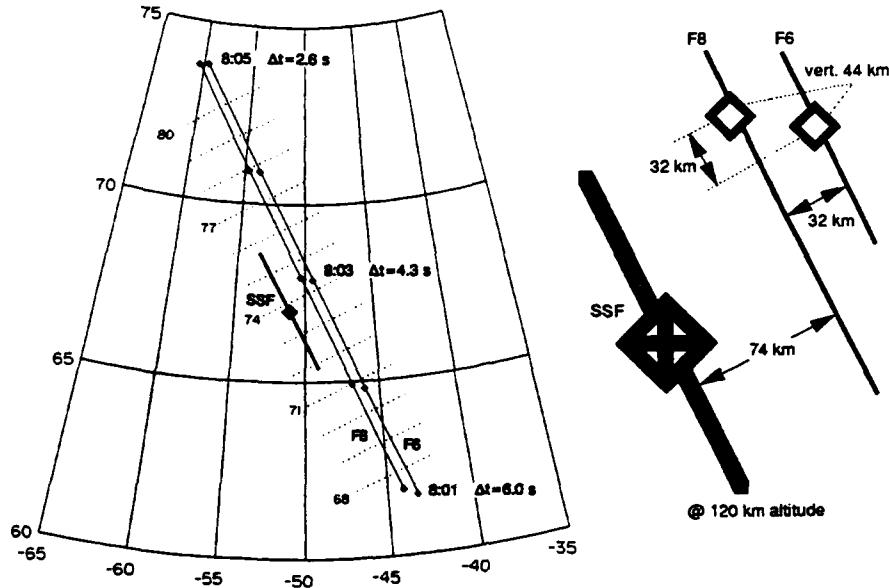


Fig. 1. Left: geographic latitude-longitude grid with the Søndrestrøm incoherent scatter radar (SSF) and its elevation scan trace (heavy), DMSP-F6 and -F8 trajectories, and invariant latitude contours (68–80°), all mapped to 120 km altitude. Δt = time difference between F6 and F8 on crossing the same invariant latitude. Right: enlarged central part of the grid including the radar location and the 0803 UT marks, showing the distances (mapped to 120 km altitude) between radar scan trace, F8 trajectory, and F6 trajectory.

difference Δt (seconds) denotes the delay between F8 and F6 on crossing the same L shell. The slightly higher F6 speed results in a shrinking lag, from $\Delta t = 6.0$ s at 0801 UT to $\Delta t = 2.6$ s at 0805 UT. On the right-hand side of Fig. 1 we have plotted an enlarged central section of the grid, showing the Søndrestrøm location with part of the scan trace and sections of the DMSP trajectories with the 0803 UT marks. At 120 km altitude, the horizontal distance along contours of constant invariant latitude is 74 km between radar scan plane and DMSP-F8 trajectory (2.4° in magnetic longitude) and 32 km between the two spacecraft trajectories (1° in magnetic longitude). The lag of $\Delta t = 4.3$ s corresponds to a latitudinal separation of 32 km (0.3°). The altitude distance between F6 and F8 was 44 km.

Figure 2 gives an overview of the DMSP-F8 particle precipitation and plasma drift measurements. We have plotted, from top to bottom, energy-time-intensity spectra of electrons and ions (particles $\text{cm}^{-2} \text{s}^{-1} \text{sr}^{-1} \text{eV}^{-1}$) and vertical and horizontal cross-track plasma drift components (m s^{-1}). Time runs from left to right, energy upward, the flux inten-

sity is color-coded (see the scaling bar on the right). The discontinuity close to the 1-keV energy level in both electron and ion spectra is artificial and caused by a mismatch between the low- and high-energy spectrometer channels at their transition point. The horizontal plasma drift is plotted in red; the westward (antisunward) velocity is positive and the eastward (sunward) negative. The vertical plasma velocity is plotted in blue, with positive meaning upward and negative downward. We have also marked the invariant latitudes (68–80°) corresponding to the interval of interest to our study. The dotted vertical line at 75.8° invariant indicates the poleward edge of the high-energy particle precipitation, which coincides with the plasma flow reversal from sunward to anti-sunward. Note, however, that the energetic particle precipitation boundary and the plasma flow reversal do not always coincide (DE LA BEAUJARDIÈRE *et al.*, 1993).

Figure 3 shows the horizontal plasma velocities in the radar scan plane (i.e. aligned with magnetic longitude) inferred from the radar scan made during the passes of the two DMSP spacecraft. Each velocity

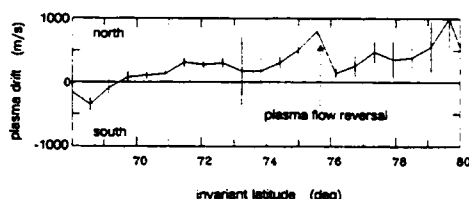


Fig. 3. Plasma drift in radar scan plane, perpendicular to the geomagnetic field and averaged over 0.6° invariant, from the radar elevation scan simultaneous with the DMSP passes (scan 2 in Fig. 6). Note the plasma flow reversal inferred from DMSP drift measurements.

estimate is obtained from several Doppler shift measurements made at various altitudes along a given magnetic field line. Between 73 and 74° invariant, where the radar beam is close to alignment with the magnetic field, the error bars become large. Otherwise the pattern is fairly stable with small error bars and shows northward velocities over most of the radar field-of-view. The velocity reaches a peak at 75.6° and drops abruptly towards the next bin at 76.2° invariant. Note that the flow reversal at 75.8° , inferred from Fig. 2 (lower panel), is located close to the peak of the northward velocity. Figure 3 seems to suggest that the reversal occurs poleward of the peak, but because the plasma velocities are averaged over 0.6° the uncertainty of the peak is $\pm 0.3^\circ$. When the velocities plotted in Fig. 3 are compared to those in Fig. 2 we notice that the east-west velocities (which exceed 1000 m s^{-1} over most of the 70 – 80° invariant latitude range and reach peaks of 2500 m s^{-1}) are significantly larger than the northward velocities except in the vicinity of the flow reversal and near 80° invariant.

By combining radar and spacecraft drift measurements (averaged over 0.6° invariant), we can construct the plasma flow pattern along the DMSP-F8 path. In so doing, we assume that the flow pattern is the same along the radar scan and the F8 trajectory (except for the altitude geometry factor) and remains constant over the few minutes it takes to complete the measurements. The result is displayed in Fig. 4 on the same latitude-longitude grid as used in Fig. 1. Following the trace from south to north, the flow orientation turns from magnetic southeastward to eastward (sunward) and rotates to westward (antisunward) in the vicinity of 76° . Poleward of the radar the velocity amplitudes are generally higher than equatorward of the radar. Such a pattern is seen very often in plasma convection measurements, see the average convection patterns (particularly the spring pattern) of DE LA BEAUJARDIÈRE *et al.* (1991).

Figure 5 shows the DMSP-F6 and -F8 measure-

ments of vertical electron and ion energy flux ($\text{eV cm}^{-2} \text{ s}^{-1} \text{ sr}^{-1} \text{ eV}^{-1}$), synchronized in invariant latitude. The range shown covers 69.5 – 79.8° invariant, as indicated by the tick marks. The central vertical thin line is only a window separator and without meaning for our discussion. In this figure, the flux parameter is different from that used in Fig. 2; there we have plotted the number flux, here the energy flux. It is obvious (and already known from earlier observations) that the F8 ion spectrometer was much noisier than the F6 instrument.

Between 71.7 and 75.8° invariant we find a structured precipitation pattern with electron energies up to 10 keV . One identifies five major bands of intense soft electron precipitation with the dominant part of the electron energy concentrated between 0.3 and 1.0 keV . The flux in the two outermost bands, around 71.8 and 74.9° invariant, is particularly intense over the energy range 30 eV – 1.2 keV . These bands are marked by open arrowheads and labeled intense low energy flux. Between them, at 74° invariant, we have placed a third open arrowhead labeled 'radar arc' whose meaning will become clear once we turn to Fig. 6. Here we only want to mention that no significant particle flux enhancement is associated with the 'radar arc'.

A comparison between absolute flux intensities from F6 and F8 is hampered by aging of the particle spectrometers and by their different noise levels; therefore, we restrict our examination to the relative flux patterns. If we compare only the relative variations in the spectra from both satellites, we notice that the large-scale patterns are similar. F6 encounters the high energy cutoff 0.15° northward of F8; this distance corresponds to 2 s flight time or two spectral measurement frames, therefore this number bears 50% uncertainty. The invariant latitudes of some small-scale intensity enhancements and depressions also do not always coincide.

When examining the gross precipitation pattern we distinguish basically three regions.

(1) Poleward of 75.8° invariant we find the lowest flux intensities; in particular, the high-energy component is missing in all channels. This is characteristic of plasma mantle precipitation.

(2) The middle part, between 71.7° invariant and the high-energy flux cutoff at 75.8° invariant, shows moderately structured electron flux with significant small-scale variations below 1 keV . The observed ion fluxes reach high intensities at keV energies. We speculate that these particles are representative for the plasma sheet boundary layer.

(3) One notices a trend toward even higher electron

Morning aurora space-time structure

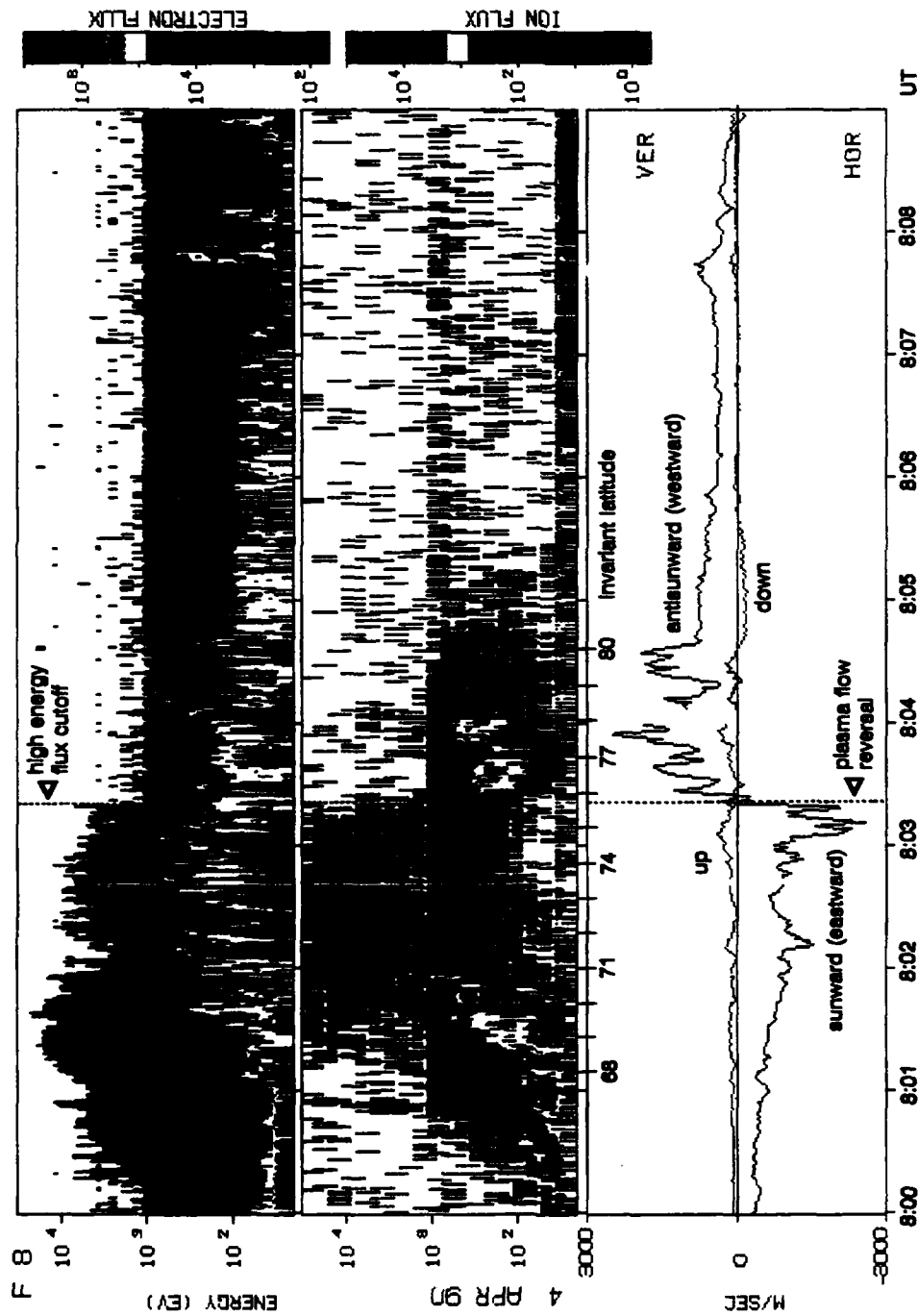


Fig. 2. DMSP-F8 measurements of the number flux of electrons (top panel) and ions (middle panel) and cross-track plasma drift (bottom panel). Universal Time and invariant latitude (at the 120 km footprint) are along the abscissa. High-energy flux cutoff and plasma flow reversal coincide.

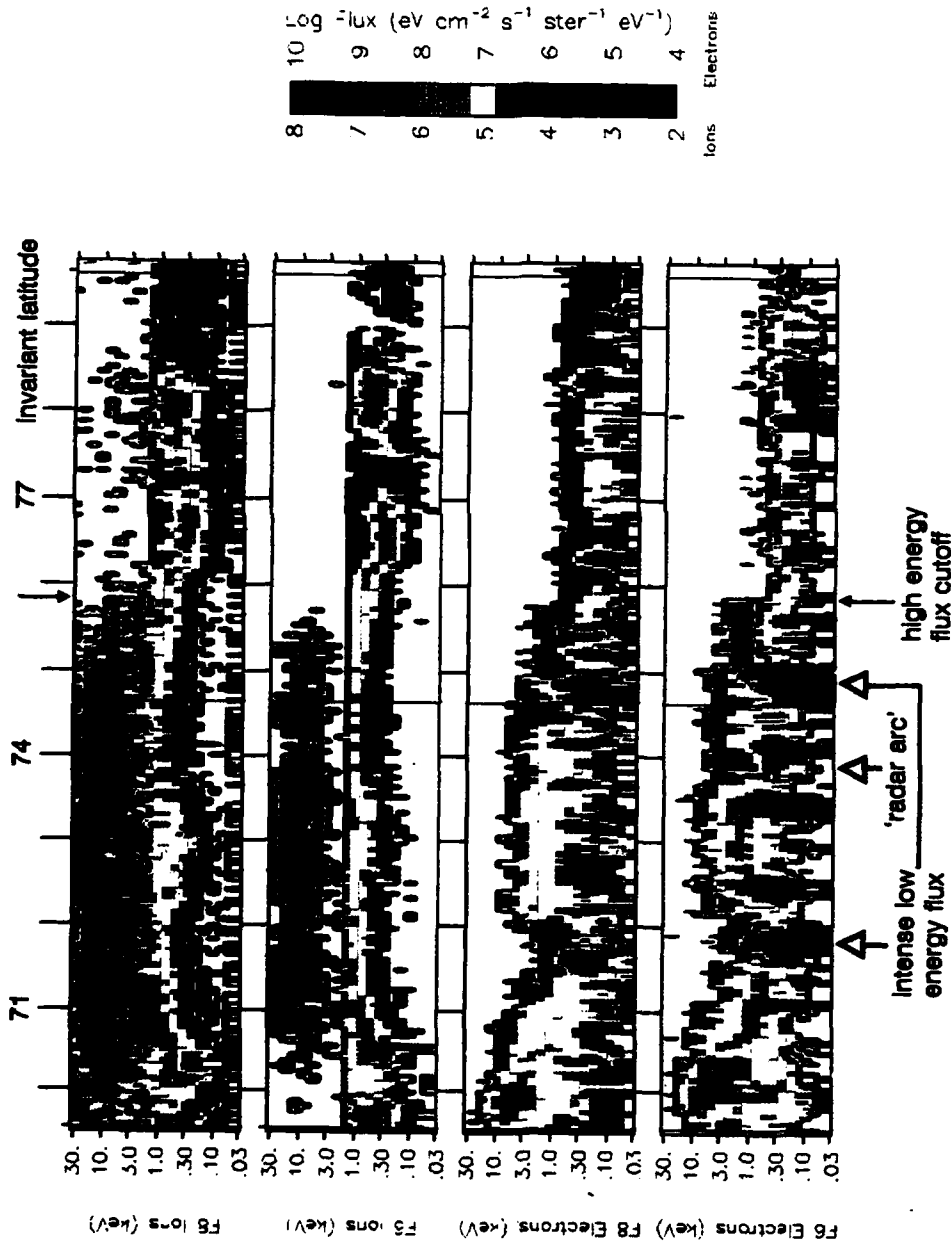


Fig. 5. Ion and electron energy flux measured onboard DMSP-F6 and -F8, synchronized in invariant latitude (tick marks on top and between the panels). From top to bottom: ions measured on F8, ions on F6, electrons on F8, and electrons on F6. The arrow labeled 'radar arc' refers to simultaneous radar observations of an auroral arc at this invariant latitude.

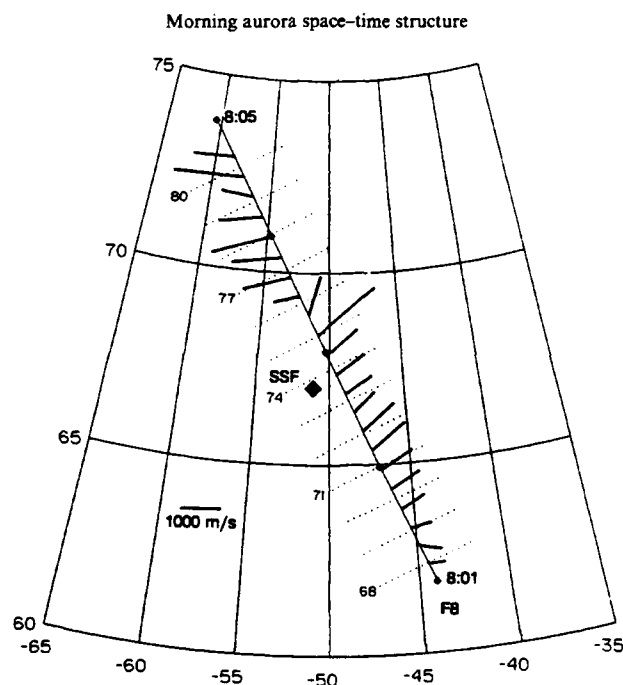


Fig. 4. Averaged plasma velocity vectors perpendicular to the geomagnetic field inferred from a combination of DMSP-F8 and radar drift measurements (Figs 2 and 3), plotted on the same grid as Fig. 1.

energies and less structured precipitation south of 71.7° invariant, accompanied by a drop-off in the high energy ion flux intensity. The diffuse character suggests precipitation of central plasma sheet particles.

Figure 6 shows the ionospheric electron density distributions measured by the incoherent scatter radar during four consecutive elevation scans, with the start times being 4.5 min apart from each other. Plotted are contours of equal electron density separated by 10^{10} m^{-3} . The scans were performed immediately before the DMSP passes (scan 1, antenna scanning from north to south), during the passes (scan 2, south to north), just after the passes (scan 3, north to south), and 9 min after the passes (scan 4, south to north). During scan 2, the radar beam was aligned with the geomagnetic field approximately at the same time the spacecraft crossed the L shell through Søndrestrøm. However, as time went on, the antenna motion lagged behind the spacecraft, such that some 80 s before the radar antenna had reached its lowest northward elevation the spacecraft field line, traced down to 120 km, passed the poleward edge of the E -region

radar field-of-view. Owing to the rotation of the Earth, the radar probed during scan 4 the same magnetic local time that the two satellites had sampled before. In other words, if one would replace the geographic grid of Fig. 1 by a geomagnetic grid, the trace of scan 4 would have been drawn between the F6 and F8 trajectories.

We have included in Fig. 6 dotted lines which correspond to the arrows plotted in Fig. 5. The arrow that was labeled 'radar arc' in Fig. 5 points to a localized region of enhanced plasma density in the upper E -layer seen during scan 2. The radar observations of this arc were made within a few seconds around the time the DMSP spacecraft measured low flux intensity at the same invariant latitude but offset by 2.4° in magnetic longitude. During scan 4, the radar detected an E -region plasma density enhancement (an auroral arc) at 74.3° invariant. This is close in latitude to the 'radar arc' of scan 2, but this arc is newly generated because enhanced plasma density at this latitude is not seen during the radar scan 3. The southernmost region of intense low-energy electron flux, at 71.7° invariant in Fig. 5, is near the equatorward edge of

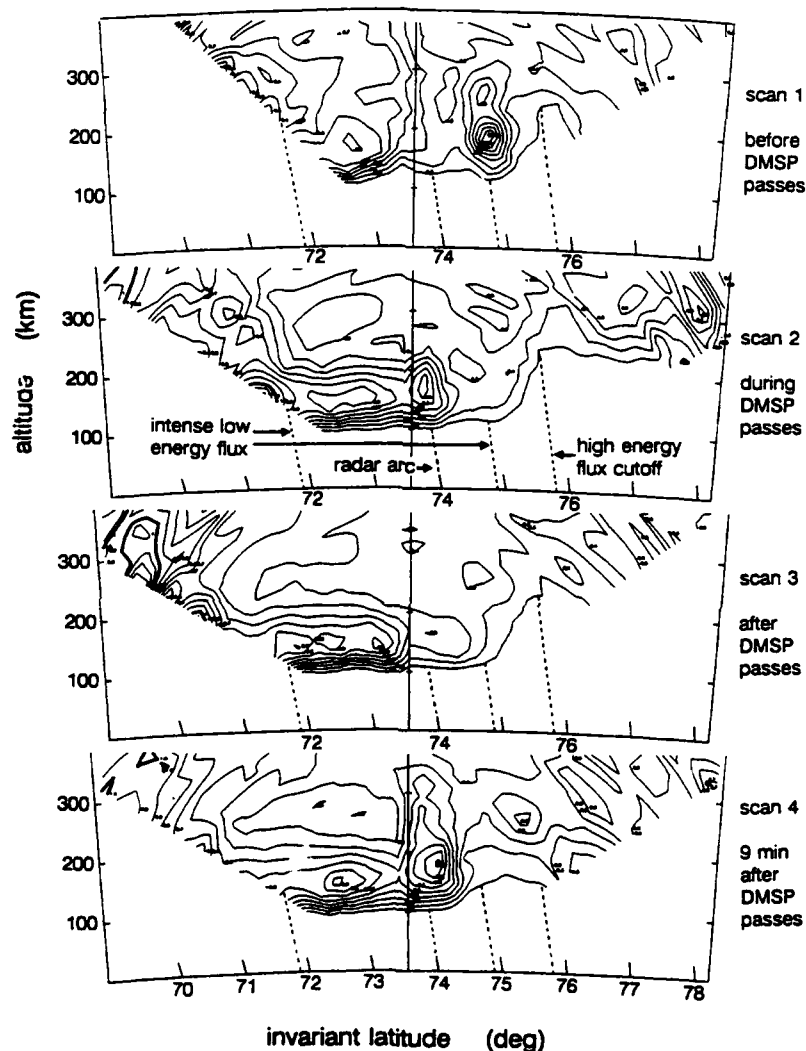


Fig. 6. Ionospheric raw plasma density profiles obtained from four consecutive radar elevation scans separated by 4.5 min. Contours of constant plasma density in steps of 10^{10} m^{-3} , beginning with $2 \cdot 10^{10} \text{ m}^{-3}$. Dotted lines correspond to the arrows in Fig. 5.

the *E*-region radar field-of-view, so that no conclusive statement about the corresponding ionospheric plasma density can be made. It appears that equatorward of 73.6° the *E*-region plasma density is enhanced in all four radar scans. This is in accordance with ionization from the 1–10 keV electron flux seen

in Fig. 5. The interval of intense low-energy flux at 74.9° invariant has no obvious counterpart in the ionospheric plasma density distribution seen during scan 2. This latitude was illuminated by the radar about 40 s after the spacecraft had passed across it. Instead, enhanced electron density is seen right at this

point during radar scan 1. The poleward boundary of the high-energy precipitation, labeled high-energy flux cutoff in Figs 4 and 5, coincides with the poleward edge of measurable *E*-region ionization during the first three scans and seems to have moved poleward by the time scan 4 was performed.

3. DISCUSSION AND CONCLUSIONS

A synoptic examination of the Søndrestrøm incoherent scatter radar and DMSP satellite observations leaves us with a situation that can be summarized as follows. We find coincidence between the reversal of the plasma flow from sunward to antisunward, the poleward boundary of energetic (>1 keV) electron and ion precipitation, and the poleward boundary of *E*-region ionization in excess of some $2 \cdot 10^{10} \text{ m}^{-3}$. The latter remained stable over the time of the first three radar scans shown in Fig. 4 (some 9 min), but varied during the preceding (not shown) and succeeding scans. We notice that the gross features of the particle precipitation observed on F6 and F8, with scale sizes exceeding one degree invariant, are similar though slightly misaligned with contours of constant invariant latitude. The small-scale structures (scale size of a fraction of one degree invariant) differ considerably more. Radar measurements made almost simultaneously with the DMSP passes show only partial coincidence between the *E*-region plasma density enhancements and the highest intensities in electron precipitation. For instance, the high *E*-region plasma density just poleward of the radar location (labeled 'radar arc') corresponds to electron flux of low intensity, and the intense soft electron flux near 74.9° invariant corresponds to low *E*-region plasma density a couple of seconds after the DMSP pass, but to high plasma density a few minutes before the pass. Between 72 and 75.8° a significant part of the electron energy flux observed on DMSP is carried by 1–10 keV electrons. More specifically, between 72.2 and 73.6° invariant a weak inverted-V structure can be identified in the F6 data, and within it slightly more of the electron energy flux is carried by the higher energy particles than is poleward of this structure. The F8 electron spectra do not show an inverted-V signature similar to that in the F6 data. The region equatorward of 73.6° invariant is in all radar scans characterized by enhanced plasma density in the lower *E*-region.

This situation suggests the following conclusions.

(1) The separation between the two DMSP spacecraft of 1° in magnetic longitude (32 km) and 4–5 s in time was too small to leave room for a significant change in the gross pattern of auroral precipitation.

The electron spectra show that the polar cap boundary, identified by the high-energy flux cutoff, was either not aligned with the *L* shell or has moved several kilometers poleward during the 4 s delay between the DMSP-F6 and -F8 measurements. A short-time fluctuation consistent with such a motion may indeed have occurred. But a steady poleward motion of the polar cap boundary over several minutes is not consistent with the radar data. The *E*-region reacts instantaneously on keV electron precipitation, and a steady motion with 1 km s^{-1} would be seen in the radar data as a shift of the *E*-region poleward boundary by several degrees invariant between scan 1 and scan 3.

(2) The 2.4° (74 km) separation between DMSP-F8 trajectory and the radar scan plane and the time lag between radar and spacecraft measurements (from 0 s at 74° to 40 s at 76° invariant) were large enough to result in significant differences between electron precipitation pattern and *E*-region plasma density enhancements.

These findings may be compared to results from Dynamics Explorer measurements obtained by THIEMAN and HOFFMAN (1985), who examined the correlation between inverted-V events observed on DE-1 and DE-2 during close-proximity passes. They found correlated events at approximately constant invariant latitude up to 18 min apart, but also the disappearance of some inverted Vs within one minute. Although the authors did not investigate the correlation span in magnetic longitude, they assumed that inverted Vs extend over a broad range of local times. Our observations in the dawn sector indicate that correlation of auroral forms including inverted Vs can cease on much smaller scales, a couple of seconds in time and 1° in magnetic longitude.

Ultraviolet auroral images from the Viking spacecraft show quite often bright spots in the dayside auroral oval, resembling beads on a string (LUI *et al.*, 1989). These bright spots were seen mostly in the afternoon sector during substorms, but at times appeared in the morning sector and during non-substorm intervals. The authors report lifetimes down to one image frame (1 min) and spatial dimensions of 50–200 km. These numbers are consistent with our data.

A possible interpretation of the observations is sketched in Fig. 7. This figure is drawn on the grid used in Fig. 1. Here we use magnetic longitude as a measure of magnetic local time. Proceeding to the left in Fig. 7 means looking at earlier and proceeding to the right means looking at later magnetic local times. Radar observations made during scan 1 will show up on the left of the diamond which marks the radar

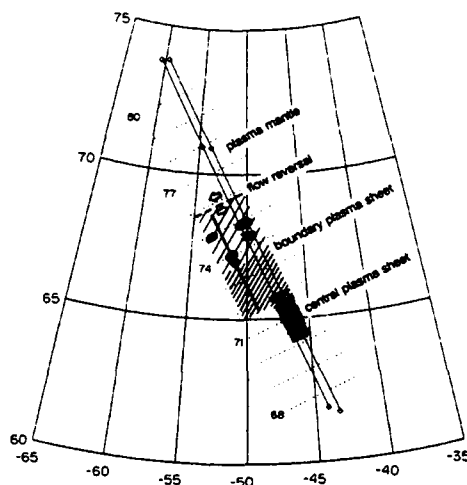


Fig. 7. A possible interpretation of the combined radar and spacecraft observations plotted on the grid used in Fig. 1. Footprints of magnetospheric regions as suggested by the DMSP and radar observations, including plasma mantle, boundary plasma sheet, and central plasma sheet. See text for details.

location, measurements during scan 2 in the vicinity of the diamond, and data from scans 3 and 4 to the right of the diamond.

We have marked by open arrows the drift orientations on both sides of the flow reversal. On the poleward side, very little precipitation was observed by the spacecraft and no significant *E*-region ionization was detected by the radar over some 15 min (equivalent to 4° magnetic longitude). This is indicative of the plasma mantle. Equatorward of the reversal, down to 71.7° invariant, we find a region where the spacecraft observed structured energetic particle precipitation (discrete arcs). The poleward section of this region is lightly hatched and corresponds to radar observations of structured, temporally variable *E*-region ionization. The equatorward section, south of 73.6° invariant, is more densely hatched to indicate the higher *E*-region plasma density throughout the four radar scans which coincides with the electron flux component of higher maximum energy. The poleward boundary of this region shifts slightly from one radar scan to the next, which is not reproduced in Fig. 7. We suggest that the particle flux between 71.7 and 75.8° invariant is characteristic of the plasma sheet boundary layer.

The localized band of enhanced particle flux recorded by DMSP near 74.9° invariant is indicated by

small concentric ovals. This spot does not extend to the left of the satellite trajectories because no arc was observed by the radar. A dark spot is placed to the left of the radar scan trace at 75° invariant. It corresponds to the region of enhanced *E*-region plasma density seen by the radar in scan 1, which is indicative of intense electron precipitation. The dark spot just north of the radar location indicates the 'radar arc', seen in scan 2 but not in scans 1 and 3 and in the particle precipitation patterns. A nearby arc appears in scan 4, 9 min later, at 74.3° invariant and is indicated by another dark spot. Finally, the intense electron flux observed by DMSP at 71.8° invariant is marked by concentric ovals across the trajectories. The radar data seem to indicate an auroral arc between 71 and 72° invariant during scan 2. But the structure appears at the equatorward edge of the *E*-region radar field-of-view, and the radar data are not conclusive. Therefore we did not extend that arc to the radar scan trace. We have examined several coincident DMSP-F7 and Søndrestrøm radar measurements which seem to indicate that a localized *E*-region plasma density enhancement frequently coincides with the poleward edge of diffuse electron precipitation.

Finally, south of 71° invariant, beyond the equatorward edge of the *E*-region radar field-of-view, we have noticed high-energy electron precipitation with energy increasing even more toward the south (see Figs 2 and 5). We have characterized this region by a densely hatched pattern in Fig. 7 and labeled it the central plasma sheet.

Although Fig. 7 provides a possible view of the auroral structure during some 15 min of radar and DMSP observations, we emphasize that our interpretation is not the only one possible. We have assumed that the pattern is static in an invariant latitude-magnetic local time frame. To assume temporal stability is probably correct for the location of the poleward boundary of particle precipitation and associated *E*-region ionization. However, it is apparently not correct with respect to details of the discrete aurora, as the comparison between DMSP particle and radar data demonstrates. The various spots, which indicate discrete auroral arcs, are most likely a result of a combination of temporal and spatial variation. This is best demonstrated by comparing the DMSP electron precipitation measurements with the radar scans 2 and 4. The 'radar arc' at 74° invariant in scan 2 appears to be coincident with weak electron precipitation at the same Universal Time but earlier magnetic local time, and the arc at 74.3° invariant seen in scan 4 corresponds to weak electron precipitation at the same magnetic local time but later Universal Time.

Morning aurora space-time structure

In concluding we emphasize that in the event discussed, the precipitation fine structure exhibits some differences between the flux measurements made by the two closely-spaced satellites, but the gross precipitation patterns appear to be similar. The spatial and temporal separation of 74 km (2.4° magnetic longitude) and 0–40 s between radar and spacecraft measurements was large enough that patterns of the discrete aurora appear to be significantly different between radar and satellite observations.

Acknowledgements—The work performed at SRI International was funded through the NSF-Søndrestrom Cooperative Agreement ATM-8822560, NSF grant ATM-9017725, and NASA contracts NASW-4399 and NASW-4603. The work performed at The Aerospace Corporation was supported by the U.S. Air Force System Command's Space System Division under contract F04701-88-C-0089. We thank D. Hardy and F. J. Rich of Phillips Laboratory and R. A. Heelis of University of Texas at Dallas for providing data from the SSJ/4 particle spectrometers and the SSIES thermal plasma experiment flown on the DMSP spacecraft.

REFERENCES

- | | | |
|---|------|--|
| DE LA BEAUJARDIÈRE O., ALCAYDE D.,
FONTANARI J. and LEGER C. | 1991 | Seasonal dependence of high-latitude electric fields. <i>J. geophys. Res.</i> 96 , 5723. |
| DE LA BEAUJARDIÈRE O., WATERMANN J., NEWELL P.
and RICH F. | 1993 | Relationship between Birkeland current regions, particle precipitation, and electric fields. <i>J. geophys. Res.</i> (in press). |
| LUI A. T. Y., VENKATESAN D. and MURPHREE J. S. | 1989 | Auroral bright spots on the dayside oval. <i>J. geophys. Res.</i> 94 , 5515. |
| KELLY J. D. | 1983 | Søndrestrom radar—initial results. <i>Geophys. Res. Lett.</i> 10 , 1112. |
| REIFF P. H., COLLIN H. L., CRAVEN J. D.,
BURCH J. L., WINNINGHAM J. D., SHELLEY E. G.,
FRANK L. A. and FRIEDMAN M. A. | 1988 | Determination of auroral electrostatic potentials using high- and low-altitude particle distributions. <i>J. geophys. Res.</i> 93 , 7441. |
| RICH F. J., HARDY D. A. and GUSSENHOVEN M. S. | 1985 | Enhanced ionosphere-magnetosphere data from the DMSP satellites. <i>Eos</i> 66 , 513. |
| RINNERT K., KOHL H., SCHLEGEL K. and
WILHELM K. | 1986 | Electric field configuration and plasma parameters in the vicinity of a faint auroral arc. <i>J. atmos. terr. Phys.</i> 48 , 867. |
| ROBINSON R. M., EVANS D. S., POTEIRA T. A. and
KELLY J. D. | 1984 | Radar and satellite measurements of an F-region ionization enhancement in the post-noon sector. <i>Geophys. Res. Lett.</i> 11 , 899. |
| ROBINSON R. M., VONDRAK R. R., HARDY D.,
GUSSENHOVEN M. S., POTEIRA T. A. and
BYTHROW P. F. | 1988 | Electrodynamics of very high latitude arcs in the morning sector auroral zone. <i>J. geophys. Res.</i> 93 , 913. |
| THIEMAN J. R. and HOFFMAN R. A. | 1985 | Determination of inverted-V stability from Dynamics Explorer satellite data. <i>J. geophys. Res.</i> 90 , 3511. |
| WICKWAR V. B., KELLY J. D.,
DE LA BEAUJARDIÈRE O., LEGER C. A.,
STEENSTRUP F. and DAWSON C. H. | 1984 | Søndrestrom overview. <i>Geophys. Res. Lett.</i> 11 , 883. |

TECHNOLOGY OPERATIONS

The Aerospace Corporation functions as an "architect-engineer" for national security programs, specializing in advanced military space systems. The Corporation's Technology Operations supports the effective and timely development and operation of national security systems through scientific research and the application of advanced technology. Vital to the success of the Corporation is the technical staff's wide-ranging expertise and its ability to stay abreast of new technological developments and program support issues associated with rapidly evolving space systems. Contributing capabilities are provided by these individual Technology Centers:

Electronics Technology Center: Microelectronics, solid-state device physics, VLSI reliability, compound semiconductors, radiation hardening, data storage technologies, infrared detector devices and testing; electro-optics, quantum electronics, solid-state lasers, optical propagation and communications; cw and pulsed chemical laser development, optical resonators, beam control, atmospheric propagation, and laser effects and countermeasures; atomic frequency standards, applied laser spectroscopy, laser chemistry, laser optoelectronics, phase conjugation and coherent imaging, solar cell physics, battery electrochemistry, battery testing and evaluation.

Mechanics and Materials Technology Center: Evaluation and characterization of new materials: metals, alloys, ceramics, polymers and their composites, and new forms of carbon; development and analysis of thin films and deposition techniques; nondestructive evaluation, component failure analysis and reliability; fracture mechanics and stress corrosion; development and evaluation of hardened components; analysis and evaluation of materials at cryogenic and elevated temperatures; launch vehicle and reentry fluid mechanics, heat transfer and flight dynamics; chemical and electric propulsion; spacecraft structural mechanics, spacecraft survivability and vulnerability assessment; contamination, thermal and structural control; high temperature thermomechanics, gas kinetics and radiation; lubrication and surface phenomena.

Space and Environment Technology Center: Magnetospheric, auroral and cosmic ray physics, wave-particle interactions, magnetospheric plasma waves; atmospheric and ionospheric physics, density and composition of the upper atmosphere, remote sensing using atmospheric radiation; solar physics, infrared astronomy, infrared signature analysis; effects of solar activity, magnetic storms and nuclear explosions on the earth's atmosphere, ionosphere and magnetosphere; effects of electromagnetic and particulate radiations on space systems; space instrumentation; propellant chemistry, chemical dynamics, environmental chemistry, trace detection; atmospheric chemical reactions, atmospheric optics, light scattering, state-specific chemical reactions and radiative signatures of missile plumes, and sensor out-of-field-of-view rejection.